EARTHQUAKE ENGINEERING AND STRUCTURAL DYNAMICS
Earthquake Engng. Struct. Dyn. **27**, 1425–1444 (1998)

EFFICIENT NON-LINEAR SEISMIC ANALYSIS OF ARCH DAMS

JOHN F. HALL*
Division of Engineering and Applied Science, California Institute of Technology, Pasadena, CA 91125, U.S.A.

SUMMARY

An approximate procedure for seismic analysis of concrete arch dams which is based on the smeared crack method is described. Features include construction sequence modelling, water and foundation interaction, crack formation, opening and closing of joints and cracks, frictional sliding, presence of shear keys, action of internal water pressure, and a reliable solution algorithm. Complete solutions can be obtained in an hour on a fast workstation computer, allowing parameter studies to be run. Results suggest that an arch dam can suffer significant cracking during strong ground shaking and still remain stable. © 1998 John Wiley & Sons, Ltd.

KEY WORDS: arch dams; non-linear analysis; cracking; joint opening; earthquake engineering

1. INTRODUCTION

Linear earthquake analysis of a concrete arch dam, conducted either in the evaluation of an existing dam or in the design of a new one, typically shows large tensile stresses when the ground motion employed represents strong shaking. *Ad hoc* procedures are needed to assess these high tensile stresses. This has spurred development of non-linear analysis capabilities that attempt to model the opening and closing of contraction joints as well as cracks that occur.

Three existing computer programs, ADAP-88 (References 1a and 1b) and the programs of References 2 and 3, represent joints and cracks by non-linear connections between the regular finite elements. Capabilities to model states of partial contact during opening and closing include a multi-layer (in the thickness direction) discretization of linearly interpolated solid and joint elements (ADAP-88), a single layer of quadratically interpolated solid and joint elements,[2] and specially calibrated joint springs connecting shell elements in a single-layer discretization.[3] Of the three approaches, ADAP-88 is the most accurate but it is also computationally intensive, as is the program of Reference 2; the program of Reference 3 is relatively efficient. Modelling sliding in joint elements is straightforward conceptually but adds to the expense and causes convergence difficulties. Only one of the approaches[2] includes features to represent sliding and its frictional aspects. The particular approach of Reference 3 does not seem amenable to being generalized to include sliding.

The procedure described here is based on the 'smeared' approach to model joints and cracks whereby the contact non-linearities are incorporated through conditions placed on the stresses at the integration points of the (shell) finite elements of the dam.[4] This approach proves to be very efficient computationally. Faster computation takes place by a reduction in the number of degrees of freedom and an improvement in convergence to the point of being able to handle frictional sliding with relative ease. The convergence is better because the variations in stiffness during transitions in contact state are smaller when the joints and cracks are smeared.

* Correspondence to: John F. Hall, Division of Engineering and Applied Science, California Institute of Technology, Mailcode 104-44, Pasadena, CA 91125, U.S.A. E-mail: johnhall@cco.caltech.edu

CCC 0098–8847/98/121425–20$17·50

Received 16 September 1997
Revised 25 February 1998

2. DESCRIPTION OF THE ANALYSIS PROCEDURE

2.1. Overview

The system analysed (Figure 1) consists of an arch dam, foundation region and water reservoir where the global co-ordinates x, y and z are in the stream, vertical and cross-stream directions, respectively. Static analysis is performed first followed by earthquake analysis. Non-linear behaviour is confined to the dam in the form of opening, closing and sliding of contraction joints and cracks. Non-linearities associated with high compressive stresses are not considered.

Static analysis simulates construction, temperature change, water level change and grouting. Each of these processes is divided into load steps. In a construction step, a specified set of elements with their gravity loads is assembled into the mesh. Each construction step can be followed by one or more temperature, water or grouting steps. In a temperature step, the elements present are subjected to a specified temperature which is assumed to vary linearly from the upstream face of the dam to the downstream face. In a water step, the water level is raised or lowered, and the elements present are subjected to the altered hydrostatic pressure. If gaps develop because of joint or crack opening at any stage of the static loading, they can be closed by the filling in of material as simulated in a grouting step. The static analysis procedure does not model processes associated with young concrete such as evolution of material properties, i.e. the same properties are used throughout the analysis.

In the static analysis, only finite element discretizations of the dam and foundation are needed since the water pressure is hydrostatic. The dam mesh is constructed of 4-node shell elements (the type with independent interpolation of translation and rotation; Reference 5) that include shear deformations. A node is located on the mid-surface and contains five degrees of freedom: two rotations about local axes and translations in the x, y and z directions. Geometry of the shell element mesh is defined through pairs of auxiliary nodes — one node on the upstream and downstream faces for each mid-surface node.

Contact non-linearities associated with the dam's joints and cracks are included through conditions on the element stresses at the integration points. While the actual interface nature of joints and cracks can only be modelled with inter-element springs, the smeared crack approach employed here is computationally more efficient and exhibits better convergence, while still giving useful results. Also, a single shell element discretization in the thickness direction of the dam is less able to represent states of partial contact than is a multi-element discretization, but it is felt to be a reasonable compromise between accuracy and computational requirements.

The foundation of the dam is elastic and is modelled with variable-node solid elements, each node containing three translational degrees of freedom. Locations of the nodes of the foundation mesh at the dam

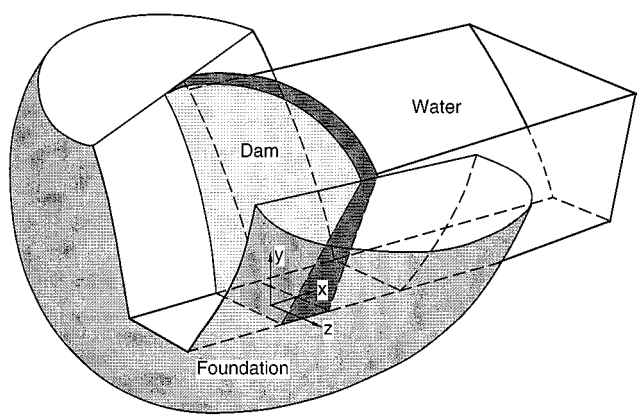

Figure 1. Arch dam with foundation and water showing coordinate system: x (stream direction), y (vertical) and z (cross-stream)

interface coincide with those of the auxiliary nodes of the dam. The foundation stiffness matrix is condensed down to the interface degrees of freedom, then transformed to the five degrees of freedom at each mid-surface node of the dam, and finally localized by zeroing all terms outside the coupling already present in the dam mesh.[3]

Each load step of the static analysis involves the iterative solution of the matrix equation of equilibrium. Time t denotes the current configuration and $t + \Delta t$ denotes the configuration after application of the next load step. The equations solved in the ℓth iteration in going from t to $t + \Delta t$ are

$$[K^{\ell} + \bar{K}]\{\Delta a^{\ell}\} = \{f(t + \Delta t)\} - \{p^{\ell}(t + \Delta t)\} - [\bar{K}]\{a^{\ell}(t + \Delta t)\} \tag{1a}$$

$$\{a^{\ell+1}(t + \Delta t)\} = \{a^{\ell}(t + \Delta t)\} + \{\Delta a^{\ell}\} \tag{1b}$$

where $[K^{\ell}]$ is the stiffness matrix of the dam which is expressed as a combination of the linear stiffness matrix $[K_{\mathrm{E}}]$ and the current tangent stiffness matrix $[K_{\mathrm{T}}^{\ell}]$, $[\bar{K}]$ is the condensed and localized stiffness matrix of the foundation, $\{f(t + \Delta t)\}$ is the static load vector containing nodal forces from gravity and from water pressure acting on the upstream dam face, $\{a^{\ell+1}(t + \Delta t)\}$ is the vector of dam displacement degrees of freedom obtained after ℓ iterations, where $\{a^{1}(t + \Delta t)\} = \{a(t)\}$, $\{\Delta a^{\ell}\}$ is the increment of dam displacements computed in the ℓth iteration; and $\{p^{\ell}(t + \Delta t)\}$ is the vector of dam forces corresponding to the stresses in state $^{\ell}(t + \Delta t)$.

Earthquake ground motions are applied after the static analysis. Components in the x, y and z directions are specified as spatially uniform. These ground motions are free-field motions that would occur at the dam–foundation interface without the dam present, and they are also applied to the floor and sides of the water reservoir. The dynamic solution is obtained from the system equation of motion which is a modification of equation (1) to include the mass of the dam, dam–water interaction, damping, and the earthquake excitation. Damping stresses in the dam are expressed as the product of a coefficient a_1 (the usual multiplier for stiffness-proportional damping) and the time rate of change of the stresses. This avoids damping stresses acting across an open joint or crack.

The equation of motion of the system is integrated using Bossak's extension[6] of Newmark's method except that a backward difference is used for the terms representing damping in the dam. The resulting equations for the ℓth iteration in going from time t to time $t + \Delta t$ are

$$\begin{bmatrix} \dfrac{(1-\alpha_{\mathrm{B}})}{\beta\Delta t^2} M + \dfrac{1}{\Delta t} C_{\mathrm{T}}^{\ell} + \dfrac{\gamma}{\beta\Delta t} \bar{C} + K^{\ell} & K_p \\ \dfrac{(1-\alpha_{\mathrm{B}})}{\beta\Delta t^2} M_p & K_{pp} \end{bmatrix} \begin{Bmatrix} \Delta a^{\ell} \\ \Delta p_{\mathrm{d}}^{\ell} \end{Bmatrix} = \begin{Bmatrix} f(t + \Delta t) \\ f_p(t + \Delta t) \end{Bmatrix}$$

$$- \begin{Bmatrix} p^{\ell}(t + \Delta t) \\ 0 \end{Bmatrix} - \begin{Bmatrix} q^{\ell}(t + \Delta t) \\ 0 \end{Bmatrix} - \begin{bmatrix} \dfrac{(1-\alpha_{\mathrm{B}})}{\beta\Delta t^2} M + \dfrac{\gamma}{\beta\Delta t} \bar{C} + \bar{K} & K_p \\ \dfrac{(1-\alpha_{\mathrm{B}})}{\beta\Delta t^2} M_p & K_{pp} \end{bmatrix} \begin{Bmatrix} a^{\ell}(t + \Delta t) \\ p_{\mathrm{d}}^{\ell}(t + \Delta t) \end{Bmatrix}$$

$$+ \begin{bmatrix} \dfrac{(1-\alpha_{\mathrm{B}})}{\beta\Delta t^2} M + \dfrac{\gamma}{\beta\Delta t} \bar{C} \\ \dfrac{(1-\alpha_{\mathrm{B}})}{\beta\Delta t^2} M_p \end{bmatrix} \{a(t)\} + \begin{bmatrix} \dfrac{(1-\alpha_{\mathrm{B}})}{\beta\Delta t} M + \left(\dfrac{\gamma}{\beta} - 1\right) \bar{C} \\ \dfrac{(1-\alpha_{\mathrm{B}})}{\beta\Delta t} M_p \end{bmatrix} \{\dot{a}(t)\}$$

$$+ \begin{bmatrix} \left(\left(\dfrac{1}{2\beta} - 1\right)(1-\alpha_{\mathrm{B}}) - \alpha_{\mathrm{B}}\right) M + \left(\dfrac{\gamma}{2\beta} - 1\right) \Delta t \bar{C} \\ \left(\left(\dfrac{1}{2\beta} - 1\right)(1-\alpha_{\mathrm{B}}) - \alpha_{\mathrm{B}}\right) M_p \end{bmatrix} \{\ddot{a}(t)\} \tag{2a}$$

$$\begin{Bmatrix} a^{\ell+1}(t + \Delta t) \\ p_{\mathrm{d}}^{\ell+1}(t + \Delta t) \end{Bmatrix} = \begin{Bmatrix} a^{\ell}(t + \Delta t) \\ p_{\mathrm{d}}^{\ell}(t + \Delta t) \end{Bmatrix} + \begin{Bmatrix} \Delta a^{\ell} \\ \Delta p_{\mathrm{d}}^{\ell} \end{Bmatrix} \tag{2b}$$

which are written in partitioned form for the displacement degrees of freedom $\{a\}$ of the dam (relative to the free-field ground motions) and the dynamic water pressure degrees of freedom $\{p_d\}$. In equation (2a), $[M]$ is the mass matrix of the dam, $[C_T^{\ell}]$ is the damping matrix of the dam and is equal to $a_1[K_T^{\ell}]$, $[\bar{C}]$ is the damping matrix of the dam foundation and is equal to $a_1[\bar{K}]$, $\{q^{\ell}(t+\Delta t)\}$ contains the nodal damping forces of the dam in state $^{\ell}(t+\Delta t)$, α_B is the Bossak parameter which can be chosen to provide high-frequency algorithmic damping, γ and β are Newmark's parameters, and $\{f(t+\Delta t)\} = \{f_{st}\} - [M][r]\{\ddot{a}_g(t+\Delta t)\}$ where $\{f_{st}\}$ is the static load vector from the dam and water, $\{\ddot{a}_g(t+\Delta t)\}$ contains the ground accelerations in the x, y and z directions, and $[r]$ is the matrix of influence vectors. Mass-proportional damping in the dam can also be added by including the term $a_0[M]$ in $[\bar{C}]$ in equation (2a), where a_0 is the usual multiplier for mass-proportional damping.

Terms $[K_{pp}]$, $[K_p]$, $[M_p]$ and $\{f_p(t+\Delta t)\}$ in equation (2a) are computed from a finite element mesh of the water and associated boundary meshes.[3] The equation representing the water is the Laplace equation with the dynamic water pressure as the unknown. Water compressibility is neglected. $[K_{pp}]$ is a condensed and localized version of the water 'stiffness' matrix which is constructed using 8-node water elements. The condensation is to the pressure degrees of freedom on the dam face, and the localization process is similar to that done for $[\bar{K}]$. Thus, the pressure-unknowns in equation (2) are only for nodes of the water mesh on the dam face. The locations of these nodes must coincide with the locations of the auxiliary dam nodes on the upstream face. In equation (2a), $[K_p]$ transforms from nodal dynamic water pressures to nodal forces on the dam; $[M_p]$ transforms from dam nodal accelerations to nodal 'forces' on the water mesh; and $\{f_p(t+\Delta t)\}$ contains the nodal 'forces' to the water mesh arising from rigid accelerations of the dam face and reservoir floor and sides at $\{\ddot{a}_g(t+\Delta t)\}$.

Vectors $\{\dot{a}(t)\}$ and $\{\ddot{a}(t)\}$ in equation (2a) are the velocity and acceleration vectors for the degrees of freedom of the dam. When convergence to $\{a(t+\Delta t)\}$ is reached, $\{\dot{a}(t+\Delta t)\}$ and $\{\ddot{a}(t+\Delta t)\}$ for use in the next time step are found from the Newmark expressions

$$\begin{aligned}\{\dot{a}(t+\Delta t)\} &= \{\dot{a}(t)\} + \{(1-\gamma)\ddot{a}(t) + \gamma\ddot{a}(t+\Delta t)\}\Delta t \\ \{\ddot{a}(t+\Delta t)\} &= \frac{1}{\beta\Delta t^2}\{a(t+\Delta t) - a(t)\} - \frac{1}{\beta\Delta t}\{\dot{a}(t)\} - \left(\frac{1}{2\beta} - 1\right)\{\ddot{a}(t)\}\end{aligned} \tag{3}$$

2.2. Details of arch dam formulation

Each shell element of the dam is mapped from a 4-node parent element as shown in Figure 2. Local co-ordinates in the parent element are ξ, η, ζ; and the ξ–η plane maps to the mid-surface of the shell where the nodes are located. Each node has five displacement degrees of freedom: translations u, v, w in the x, y, z directions, respectively, and rotations θ and γ about axes $\hat{x}$ and $\hat{y}$, respectively, that are local to each node. The $\hat{x}$- and $\hat{y}$-axis at a node are perpendicular to the mapped ζ direction which is the $\hat{z}$-axis. The $\hat{x}$-axis is in the $y \times \hat{z}$ direction, and so is in the horizontal plane; $\hat{y}$ is the $\hat{z} \times \hat{x}$ direction. At each mid-surface node, the intersections of the $\hat{z}$ axis with the upstream and downstream faces of the dam locate the auxiliary nodes.

Stresses in a shell element are referenced to local 1, 2, 3 co-ordinates: 1 is horizontal in the mapped ξ–η plane and is oriented so that its z component is negative; 2 is in the same plane and perpendicular to 1; and 3 is the 1×2 direction. Thus, the directions 1 and 2 can be associated with arch and cantilever actions, respectively. Normal stress components (tension positive) are σ_{11} (arch) and σ_{22} (cantilever); the through-thickness normal stress component σ_{33} is set to zero. Shear stress components are τ_{12} (in-plane shear), τ_{23} (out-of-plane cantilever shear) and τ_{13} (out-of-plane arch shear). A positive τ_{ij} stretches the bisector of the right angle formed by the positive i- and j-axis. Corresponding strain components are denoted as $\varepsilon_{11}, \varepsilon_{22}, \varepsilon_{33}, \gamma_{12}, \gamma_{23}$ and γ_{13}. Within each element a single set of 1, 2, 3 directions is used, and these directions are evaluated at the element centre.

Non-linear features of element behaviour are associated with contact and sliding in the contraction joints and cracks. Actions at these locations are represented through conditions placed on the stresses at discrete

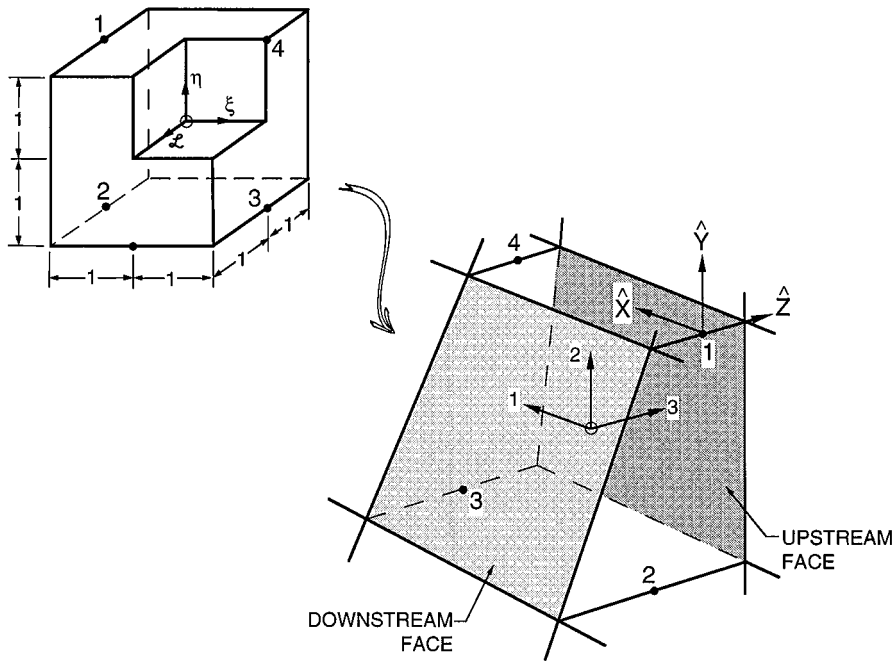

Figure 2. Shell element of an arch dam shown mapped from a parent element

points within the element used to evaluate element integrands. At each integration point, the orientation of the contraction joint is that of the 2–3 plane, while the orientation of the cracking plane is that of the 1–3 plane. The contraction joints are assumed to have zero tensile strength, and so

$$\begin{aligned} \sigma_{11} &= 0 \text{ for joint open} \\ &< 0 \text{ for joint closed} \end{aligned} \tag{4}$$

Crack formation on a cracking plane employs a simple strength criterion. Before cracking,

$$\sigma_{22} < \sigma_{\text{ten}} \tag{5}$$

where σ_{ten} is the tensile strength of the cracking plane. Cracking occurs when σ_{22} reaches σ_{ten}, upon which σ_{ten} is set to zero. After cracking,

$$\begin{aligned} \sigma_{22} &= 0 \quad \text{for crack open} \\ &< 0 \quad \text{for crack closed} \end{aligned} \tag{6}$$

Shear stresses in the contraction joints and cracks are limited by simple friction criteria:

$$|\tau_{13}| \leqslant f_1|\sigma_{11}| \tag{7a}$$

$$|\tau_{23}| \leqslant f_2|\sigma_{22}| \quad \text{if crack is present} \tag{7b}$$

$$\left.\begin{aligned} |\tau_{12}| &\leqslant \tfrac{1}{2}(f_1|\sigma_{11}| + f_2|\sigma_{22}|) \quad \text{if crack is present} \\ \alpha_s \cdot G \cdot \gamma_{12} - f_1|\sigma_{11}| \leqslant \tau_{12} &\leqslant \alpha_s \cdot G \cdot \gamma_{12} + f_1|\sigma_{11}| \quad \text{if crack is not present} \end{aligned}\right\} \tag{7c}$$

where f_1 and f_2 are friction coefficients for contraction-joint and crack shear, respectively, α_s is a shear stiffness retention factor, G is the shear modulus, and $<$ or $>$ applies when sliding is not occurring, and $=$ holds

for sliding. These relations imply that there are three uncoupled sliding mechanisms. The $\alpha_s \cdot G \cdot \gamma_{12}$ term retains some stiffness in the 12 component prior to cracking when the joint is open.

The current contact state is defined by the current tensile strength σ_{ten} of the cracking plane and by a contact descriptor L_{CON}. The current value of σ_{ten} indicates whether a crack has formed ($=0$) or not (>0). Four contact states are possible as follows:

$$\begin{aligned} L_{CON} = 1: &\quad \text{both joint and cracking plane open} \\ = 2: &\quad \text{joint closed, cracking plane open} \\ = 3: &\quad \text{joint closed, no crack or cracking plane closed} \\ = 4: &\quad \text{joint open, no crack or cracking plane closed} \end{aligned} \tag{8}$$

The current sliding state is defined by $L_{SLD}ij$ where ij take on values 12, 23 and 13 corresponding to the three shear components. In general, $L_{SLD}ij = 0$ if sliding is not occurring for the shear component ij and is $\neq 0$ if sliding is occurring, being <0 if $\tau_{ij} < 0$ and >0 if $\tau_{ij} \geqslant 0$.

In each element, the stresses and strains as well as values of σ_{ten}, L_{CON}, $L_{SLD}12$, $L_{SLD}23$, $L_{SLD}13$ are kept track of at the integration points. The particular integration scheme employed uses four points located at $\xi, \eta, \zeta = 0, 0, 1;\ 0, 0, \frac{1}{3};\ 0, 0, -\frac{1}{3};\ 0, 0, -1$. Weighting values are 1 for the two exterior points and 3 for the two interior points. The four-point integration scheme is used to integrate the element tangent stiffness matrix $[K_T^\ell]^e$ and the element right-side vectors $\{p^\ell(t+\Delta t)\}^e$ and $\{q^\ell(t+\Delta t)\}^e$. Formulas for the element quantities are

$$[K_T^\ell]^e = \int_{v^e} [B^e]^T [D_T^\ell][B^e]\, dv^e \tag{9}$$

$$\{p^\ell(t+\Delta t)\}^e = \int_{v^e} [B^e]^T \{\sigma^\ell(t+\Delta t)\}^e\, dv^e \tag{10}$$

$$\{q^\ell(t+\Delta t)\}^e = \int_{v^e} [B^e]^T \{\hat{\sigma}^\ell(t+\Delta t)\}^e\, dv^e \tag{11}$$

where v^e is the element domain, $\{\sigma^\ell(t+\Delta t)\}^e$ lists the element stresses, $[B^e]$ transforms from element displacements $\{a\}^e$ to element strains $\{\varepsilon\}^e$; $[D_T^\ell]$ is the tangent material matrix which relates element strain increments $\{d\varepsilon^\ell\}^e$ to element stress increments $\{d\sigma^\ell\}^e$, $\hat{}$ denotes damping stress, and the element stresses and strains are listed in the order 11, 22, 12, 23, 13. With Young's modulus E and Poisson's ratio v, the non-zero values in $[D_T^\ell]$ are given by

$$\begin{aligned} D_T^\ell(1,1) &= E \text{ if } L_{CON} = 2;\ = E/(1-v^2) \text{ if } L_{CON} = 3 \\ D_T^\ell(1,2) &= D_T^\ell(2,1) = Ev/(1-v^2) \text{ if } L_{CON} = 3 \\ D_T^\ell(2,2) &= E \text{ if } L_{CON} = 4;\ = E/(1-v^2) \text{ if } L_{CON} = 3 \\ D_T^\ell(3,i) &= \mp \tfrac{1}{2}(f_1 \cdot D_T^\ell(1,i) + f_2 \cdot D_T^\ell(2,i)) \text{ if } L_{SLD}12 \gtrless 0 \text{ and } \sigma_{ten} = 0 \\ &= \mp f_1 \cdot D_T^\ell(1,i) \text{ if } L_{SLD}12 \gtrless 0 \text{ and } \sigma_{ten} > 0: \quad i = 1,2 \\ D_T^\ell(3,3) &= G \text{ if } L_{SLD}12 = 0 \\ &= \alpha_s \cdot G \text{ if } L_{SLD}12 \neq 0 \quad \text{and} \quad \sigma_{ten} > 0 \\ D_T^\ell(4,i) &= \mp f_2 \cdot D_T^\ell(2,i) \text{ if } L_{SLD}23 \gtrless 0: \quad i = 1,2 \\ D_T^\ell(4,4) &= G' \text{ if } L_{SLD}23 = 0 \\ D_T^\ell(5,i) &= \mp f_1 \cdot D_T^\ell(1,i) \text{ if } L_{SLD}13 \gtrless 0: \quad i = 1,2 \\ D_T^\ell(5,5) &= G' \text{ if } L_{SLD}13 = 0 \end{aligned} \tag{12}$$

where $G' = \frac{5}{6}G$ (the usual correction for out-of-plane shear). The values that result from $L_{\mathrm{CON}} = 3$ and $L_{\mathrm{SLD}}12 = L_{\mathrm{SLD}}23 = L_{\mathrm{SLD}}13 = 0$ give the linear material matrix $[D_{\mathrm{E}}]$ which leads to the linear stiffness matrix $[K_{\mathrm{E}}]^e$.

Following the solution of equation (1a) or (2a) for the incremental displacements $\{\Delta a^{\ell}\}$ of the dam, the state $^{\ell}(t + \Delta t)$ is updated to the state $^{\ell+1}(t + \Delta t)$ at each integration point. This process begins by determining the element strain increments from

$$\{\Delta\varepsilon^{\ell}\}^e = [B^e]\{\Delta a^{\ell}\}^e \tag{13}$$

and then updating the strains as

$$\{\varepsilon^{\ell+1}(t + \Delta t)\}^e = \{\varepsilon^{\ell}(t + \Delta t)\}^e + \{\Delta\varepsilon^{\ell}\}^e \tag{14}$$

The normal stresses $\sigma_{11}^{\ell+1}(t + \Delta t)$ and $\sigma_{22}^{\ell+1}(t + \Delta t)$ depend only on the normal strains $\varepsilon_{11}^{\ell+1}(t + \Delta t)$ and $\varepsilon_{22}^{\ell+1}(t + \Delta t)$. For each of the four contact conditions:

$$\begin{aligned}
\sigma_{11}^{\ell+1}(t + \Delta t) &= 0 \text{ for } L_{\mathrm{CON}} = 1 \text{ or } 4 \\
&= E \cdot \varepsilon_{11}^{\ell+1}(t + \Delta t) \text{ for } L_{\mathrm{CON}} = 2 \\
&= \frac{E}{1 - v^2} \cdot (\varepsilon_{11}^{\ell+1}(t + \Delta t) + v \cdot \varepsilon_{22}^{\ell+1}(t + \Delta t)) \text{ for } L_{\mathrm{CON}} = 3
\end{aligned} \tag{15a}$$

$$\begin{aligned}
\sigma_{22}^{\ell+1}(t + \Delta t) &= 0 \text{ for } L_{\mathrm{CON}} = 1 \text{ or } 2 \\
&= \frac{E}{1 - v^2} \cdot (v \cdot \varepsilon_{11}^{\ell+1}(t + \Delta t) + \varepsilon_{22}^{\ell+1}(t + \Delta t)) \text{ for } L_{\mathrm{CON}} = 3 \\
&= E \cdot \varepsilon_{22}^{\ell+1}(t + \Delta t) \text{ for } L_{\mathrm{CON}} = 4
\end{aligned} \tag{15b}$$

Each of the four contact states occupies a sector in $\varepsilon_{11} - \varepsilon_{22}$ space (numbered 1, 2, 3 and 4 to coincide with the value of L_{CON}); the diagram differs depending on whether a crack has not formed (Figure 3(a)) or has formed (Figure 3(b)). Should the strain location $\varepsilon_{11}^{\ell+1}(t + \Delta t)$, $\varepsilon_{22}^{\ell+1}(t + \Delta t)$ move above the top line in Figure 3(a), indicating the formation of a crack, then σ_{ten} is set to zero and Figure 3(b) is used thereafter. L_{CON} takes the number of the sector in which $\varepsilon_{11}^{\ell+1}(t + \Delta t)$, $\varepsilon_{22}^{\ell+1}(t + \Delta t)$ resides.

Updating a shear stress requires integration over the strain increment path. A trial value of shear stress is obtained assuming linear behaviour over the increment, and then the trial stress is scaled back if needed to satisfy equation (7). A shear stress that needs to be scaled back means that sliding is present. In the procedure, the strain increment is divided into segments in order to account for spanning multiple sectors and/or a cracking event. As an example, consider computation of $\tau_{12}^{\ell+1}(t + \Delta t)$ for a strain increment $\Delta\gamma_{12}^{\ell}$. The result also depends on the strain increments $\Delta\varepsilon_{11}^{\ell}$ and $\Delta\varepsilon_{22}^{\ell}$ which are shown in Figure 3 as the path from a to d. (Point a is $\varepsilon_{11}^{\ell}(t + \Delta t)$, $\varepsilon_{22}^{\ell}(t + \Delta t)$ and point d is $\varepsilon_{11}^{\ell+1}(t + \Delta t)$, $\varepsilon_{22}^{\ell+1}(t + \Delta t)$.) Four segments are necessary: ab, bc, cc' (cracking event) and $c'd$. $L_{\mathrm{SLD}}12$ is updated according to the action taken in the last segment.

After the stresses are updated, the updated damping stresses are found from

$$\{\hat{\sigma}^{\ell+1}(t + \Delta t)\}^e = \frac{a_1}{\Delta t}\{\sigma^{\ell+1}(t + \Delta t) - \sigma(t)\}^e \tag{16}$$

The mass matrix $[M]$ of the dam in equation (2a) is assembled from element mass matrices $[M]^e$, computed for mass lumped at the eight auxiliary node locations in each element. This mass lumping removes coupling of inertial forces across the contraction joints and cracks.

The static loading from a temperature step is incorporated in equation (1a) through a modification of the stress calculation which affects $\{p^{\ell}(t + \Delta t)\}$ through equation (10). If a temperature change ΔT (positive for temperature increase) is specified for step t to $t + \Delta t$, the sector diagram (including the cracking line) is shifted

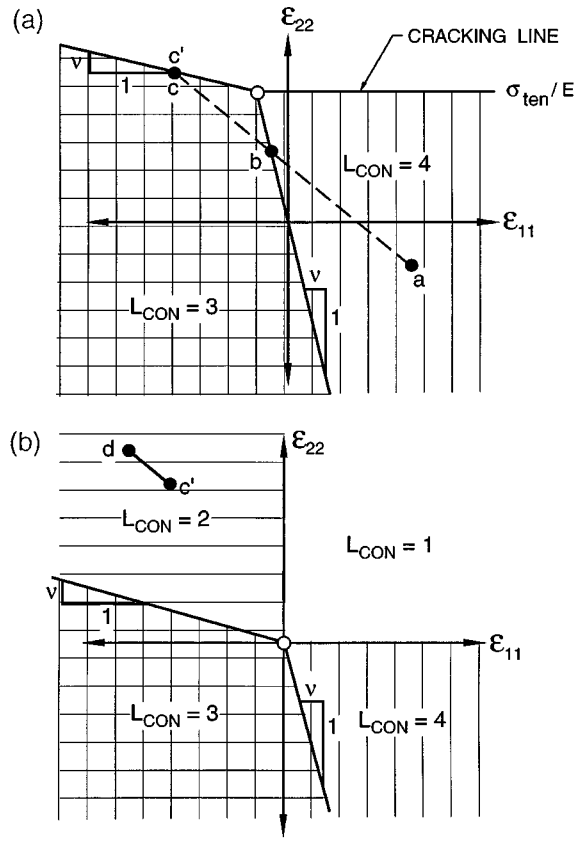

Figure 3. Division of ε_{11}–ε_{22} space into sectors corresponding to specific contact states when a contraction joint is present. The line from a to d represents a strain path. (a) Sector diagram before cracking; (b) Sector diagram after cracking

relative to the strain axes by amounts $\alpha_1 \Delta T$ and $\alpha_2 \Delta T$ along the ε_{11} and ε_{22} axes, respectively, where α_1 and α_2 are coefficients of thermal expansion in directions 1 and 2, respectively. This is shown in Figure 4(a) which is based on Figure 3(b). The initial strain state $\varepsilon^1_{11}(t + \Delta t)$, $\varepsilon^1_{22}(t + \Delta t)$ is not affected, although the sector in which the strain state resides might change. The stresses $\sigma^1_{11}(t + \Delta t)$ and $\sigma^1_{22}(t + \Delta t)$, which would be the converged values $\sigma_{11}(t)$ and $\sigma_{22}(t)$ from the previous load step, are recomputed using strains measured from the origin of the shifted sector diagram; i.e., the strains in equation (15) are replaced by $\varepsilon^1_{11}(t + \Delta t) - \alpha_1 \Delta T$ and $\varepsilon^1_{22}(t + \Delta t) - \alpha_2 \Delta T$. The shear stresses $\tau^1_{12}(t + \Delta t)$, $\tau^1_{23}(t + \Delta t)$ and $\tau^1_{13}(t + \Delta t)$ are taken as the previously converged values $\tau_{12}(t)$, $\tau_{23}(t)$ and $\tau_{13}(t)$, but subject to the scaling back operation if equation (7) is not satisfied with the recomputed $\sigma^1_{11}(t + \Delta t)$ and $\sigma^1_{22}(t + \Delta t)$. With these new stresses, $\{p^1(t + \Delta t)\}$ is computed from equation (10) and equation (1) is solved at $\ell = 1$; iterations continue until convergence. For each iteration and in subsequent load steps, stresses are computed using the shifted sector diagrams. Future temperature load steps cause additional shifts in the sector diagrams.

A grouting step in the static analysis to fill in gaps in the contraction joints and cracks also involves shifting the sector diagram, additive to those shifts resulting from temperature steps and previous grouting steps. If the current strain resides in sector 1 or 4, then the open contraction joint is 'filled in' by shifting the sector diagram to the right by an amount $\Delta\varepsilon^{op}_{11}$ until the right edge of sector 2 or 3 intersects the strain location (Figures 4(b) and (d)). If the current strain resides in sector 1 or 2, then the open crack is 'filled in' by shifting the sector diagram upward by an amount $\Delta\varepsilon^{op}_{22}$ until the top edge of sector 3 or 4 intersects the strain location (Figures 4(c)

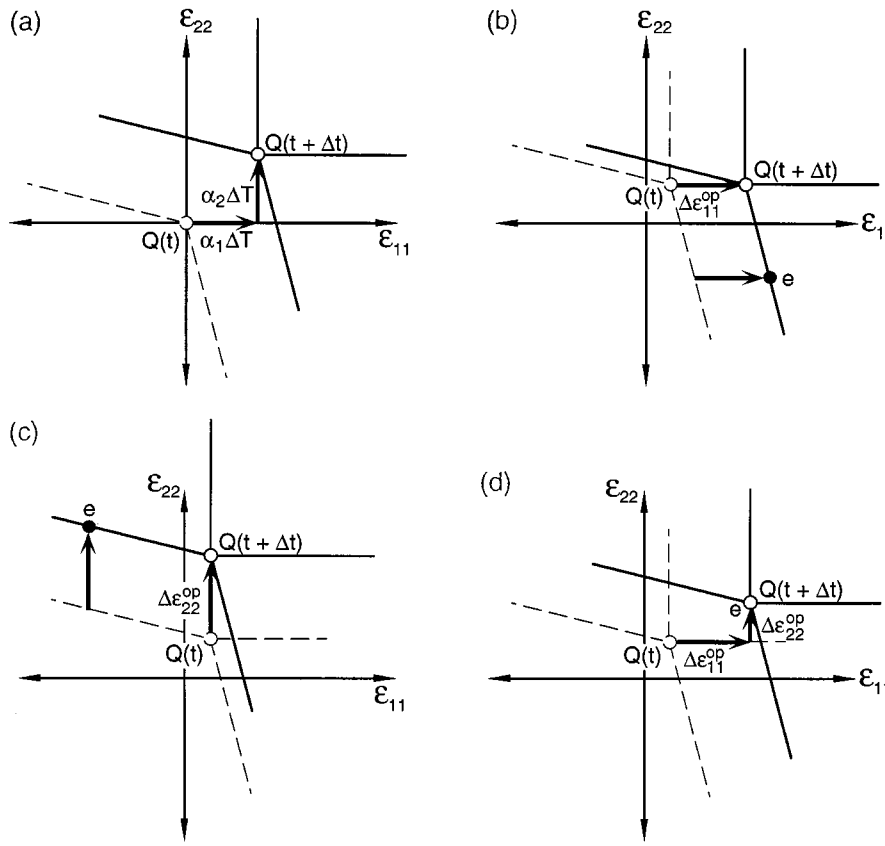

Figure 4. Shifts in sector diagram caused by (a) temperature shift of previously unshifted sector diagram; (b) grouting shift of previously shifted sector diagram to close a joint; (c) grouting shift of previously shifted sector diagram to close a crack; and (d) grouting shift of previously shifted sector diagram to close a joint and a crack. Point Q marks the origin of the sector diagram. Point e represents a strain state containing an open joint and/or crack that is/are closed by grouting. The sector diagram shown is for both contraction joint and crack present

and (d)). In neither case do the stresses change, and no solutions of equation (1a) are required. The shifted sector diagrams are used in all subsequent stress calculations.

2.3. *Convergence issues*

Convergence over iterations in a load or time step is attained when the maximum force and moment residuals, absolute values denoted by $F^{\ell}_{\max}$ and $M^{\ell}_{\max}$ and taken from the residual vector for the ℓth iteration (the right-hand side of equation (1a) or (2a)), are reduced below specified tolerances. A proper choice of the iterating stiffness matrix $[K^{\ell}]$ in equation (1a) or (2a) is necessary so that the iterations in each load or time step converge within a reasonable computational effort. This matrix is taken to be a combination of $[K_{\mathrm{E}}]$, the linear stiffness matrix for the dam as an elastic monolithic structure, and $[K^{\ell}_{\mathrm{T}}]$, the tangent stiffness matrix representing the contact and sliding non-linearities in the $^{\ell}(t + \Delta t)$ state, as follows:

$$[K^{\ell}] = S^{\ell} \cdot [K_{\mathrm{E}}] + (1 - S^{\ell}) \cdot [K^{\ell}_{\mathrm{T}}] \tag{17}$$

The parameter S^ℓ is selected according to an algorithm that makes use of $F^\ell_{\max}$ and $M^\ell_{\max}$:

For the first iteration ($\ell = 1$), set S^1 equal to a 'safe' value $S_{\max} \leqslant 1$. The closer $S_{\max}$ is to one, the closer $[K^\ell]$ is to the 'safe' matrix $[K_E]$.

For subsequent iterations ($\ell > 1$), set

$$\begin{aligned} S^\ell &= S_{\max} \text{ if } F^\ell_{\max} > 1{\cdot}1 \cdot F^{\ell-1}_{\max} \\ &= S^{\ell-1} \text{ if } F^\ell_{\max} < 0{\cdot}7 \cdot F^{\ell-1}_{\max} \text{ or } M^\ell_{\max} < 0{\cdot}7 \cdot M^{\ell-1}_{\max} \\ &= S^{\ell-1}/2 \text{ otherwise, but with some lower limit } S_{\min} \end{aligned}$$

Thus, as the iterations proceed, S^ℓ is reduced as convergence slows, bringing the iterating matrix closer to the current tangent, but S^ℓ is returned to the 'safe' value $S_{\max}$ should the residual jump up significantly.

Even with the above algorithm for selecting $[K^\ell]$, convergence still occasionally proceeds very slowly or even stops if the computations get stuck in a loop and repeat every so many iterations. This can usually be attributed to the occurrence of frictional sliding in the elements. For situations in which convergence does not occur within a specified number of iterations, automatic division of the load or time step is employed. Convergence difficulties are most often encountered during the static analysis, especially with the construction and temperature steps. In the dynamic analysis, the smoothing effect of inertia and damping terms aids convergence.

The other issue of convergence is how small must the time step Δt be so that a converged solution is obtained over the complete set of time steps. This is discussed further in Section 3.

2.4. Additional features of dam model

An option is included to omit the contraction joint from an element. In the formulation, equations (4) and (7a) are ignored; equation (7c) is replaced by

$$\alpha_s \cdot G \cdot \gamma_{12} - f_2 |\sigma_{22}| \leqslant \tau_{12} \leqslant \alpha_s \cdot G \cdot \gamma_{12} + f_2 |\sigma_{22}| \quad \text{if crack is present} \tag{7c'}$$

equation (12) for the tangent material matrix is changed appropriately; and $L_{SLD}13 = 0$. Applicable sector diagrams contain only sectors corresponding to $L_{CON} = 2$ and 3. One use for this option is that its selection for every element, along with a high tensile strength for the cracking planes, produces linear behaviour.

Another option is intended to simulate a keying action such as produced by shear keys in the contraction joints and by rough surfaces of the cracking planes. A keyed condition that allows opening but no sliding can be applied to each of the three shear components as desired. The appropriate parts of equation (7) are not enforced and the appropriate $L_{SLD}ij$ stay at zero. Keying is assumed to be present even when a contraction joint or crack is completely open.

Once the first integration point of an element cracks, a third option facilitates crack extension through the dam by reducing the cracking strength at the other three integration points to some specified value σ^{red}_{ten}. Because of the linear stress distribution through the thickness of the dam, the first integration point of an element to crack will always be the one on either the upstream or downstream face. Once this crack forms, the use of the full tensile strength at the other integration points ahead of the crack tip would be too restrictive regarding crack propagation.

Another option related to cracking is to spread out the interval of time over which stresses are released once cracking occurs at an integration point. This may be more realistic and it also improves some aspects of the numerical behaviour. When the cracking strength is reached at an integration point, say at time t_c, the stresses to be released (denoted by $\{\sigma_c\}^e$) are computed as discussed in Section 2.2 for a cracking event. To spread the stress release out over some finite time interval T_r, the stresses $\{\sigma'(t + \Delta t)\}^e$ in equation (10), computed as before assuming instantaneous stress release, are augmented by the term $\{\sigma_c\}^e \cdot c(t)$, where $c(t)$ varies linearly from one at $t = t_c$ to zero at $t = t_c + T_r$ and remains at zero for $t > t_c + T_r$.

A final feature pertains to water pressure loads on the dam. The loading discussed in Section 2.1 is for water pressure acting on the upstream dam face, both static and dynamic components. Water pressure can also act internally in the pores of the concrete as well as on the faces of contraction joints and cracks if water penetration occurs. While the static problem is tractable, the dynamic one is very complicated and even approximate treatment is probably not feasible. The approach here is to make some simple calculations of the internal pressures $p'_{11}(t+\Delta t)$ and $p'_{22}(t+\Delta t)$ in directions 1 and 2 at each integration point, and then to add these pressures (compression being negative) to the stresses $\sigma'_{11}(t+\Delta t)$ and $\sigma'_{22}(t+\Delta t)$ in equation (10). For the static case, whether or not contraction joints or cracks are present

$$p'_{11}(t+\Delta t) = p'_{22}(t+\Delta t) = \frac{1+\zeta}{2}\left\langle \frac{1}{4}\frac{1}{4}\frac{1}{4}\frac{1}{4} \right\rangle \{p_s\}^e \tag{18}$$

which corresponds to a linear variation in pressure through the dam thickness from the static water pressure at the upstream face (nodal values in $\{p_s\}^e$) to zero at the downstream face. In the dynamic case, this expression is still used for $p'_{11}(t+\Delta t)$ if a contraction joint is not present and for $p'_{22}(t+\Delta t)$ if a crack is not present. In the dynamic case if a joint is present

$$p'_{11}(t+\Delta t) = \frac{1+\zeta}{2}\left\langle \frac{1}{4}\frac{1}{4}\frac{1}{4}\frac{1}{4} \right\rangle \{p_s + p'_d(t+\Delta t)\}^e \tag{19a}$$

and if a crack is present

$$p'_{22}(t+\Delta t) = \frac{1+\zeta}{2}\left\langle \frac{1}{4}\frac{1}{4}\frac{1}{4}\frac{1}{4} \right\rangle \{p_s + p'_d(t+\Delta t)\cdot(1-c(t))\}^e \tag{19b}$$

which are written for the total water pressure (static and dynamic values in $\{p_s\}^e$ and $\{p'_d(t+\Delta t)\}^e$, respectively).

When the internal dynamic pressure is included, a tangent contribution is added to $[K_p]$ in equation (2a) which is assembled from element matrices

$$[K_{ip}]^e = \int_{v^e} \{b_1 + b_2\cdot(1-c(t))\}^e \frac{1+\zeta}{2}\left\langle \frac{1}{4}\frac{1}{4}\frac{1}{4}\frac{1}{4} \right\rangle \mathrm{d}v^e \tag{20}$$

integrated by the 4-point scheme. In equation (20), $\{b_1\}^e$ and $\{b_2\}^e$ are the first two columns of $[B^e]^T$; $\{b_1\}^e$ is included only if a contraction joint is present, and $\{b_2\}^e$ is included only if a crack is present.

2.5. *Discussion of assumptions*

A dam–water–foundation system subjected to strong earthquake shaking is a complex situation, and numerous assumptions are necessary to replace the actual system with one that can be analysed. In such a process, it is important to understand the severity of the assumptions regarding accuracy of the computed results. Therefore, discussion of the assumptions used in the computer program is presented below.

The treatment of the free-field ground motions along the dam and water boundaries as spatially uniform is far from reality as shown most recently by the accelerograms recorded at Pacoima Dam during the Northridge earthquake.[7] Studies[8] show that nonuniformity in ground motion is an important parameter and that the assumption of uniformity can be either conservative or unconservative. The major difficulty is not so much in the formulation but in defining the nonuniformity itself, and this is an issue that needs more study. Therefore, in this first version of the computer program, the treatment of seismic input is limited to the simple case of uniform free-field motion.

An assumption associated with modelling the water is that of incompressibility. Including water compressibility would significantly increase the cost of the analysis, and while water compressibility effects are known to be important for some dams, this is probably not a major limitation of the program. One ongoing study of

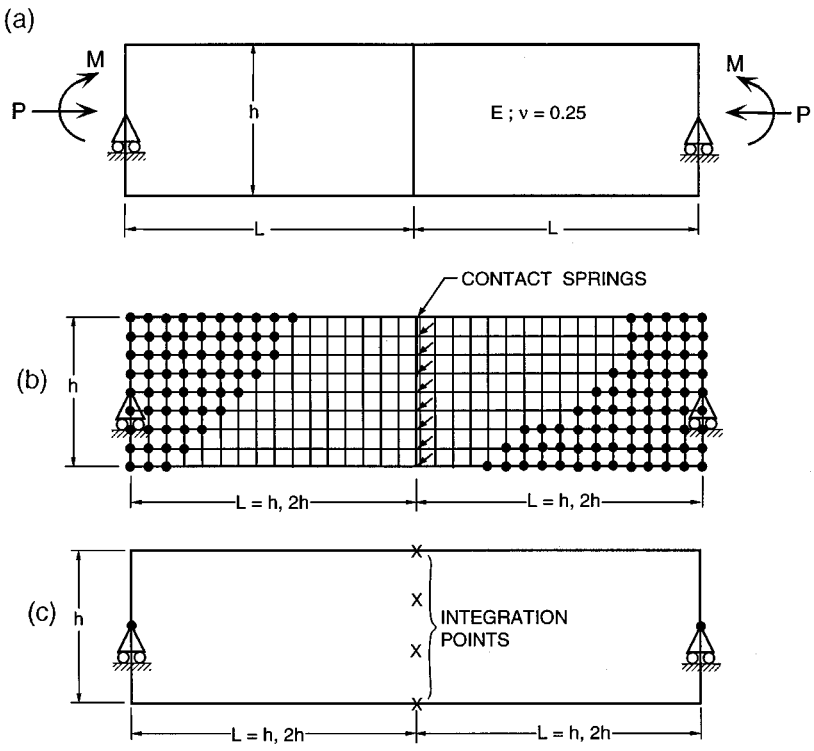

Figure 5. Problem of (a) a plane-strain beam with centre joint. Discrete versions by (b) finite element mesh of 4-node, plane-strain elements with contact springs in centre joint and (c) single plane-strain beam element with smeared cracking at integration points along pre-cracked centre joint

Morrow Point Dam,[9] where water compressibility effects are thought to play an important role in the dynamic response, has not been successful in reproducing the results of carefully controlled force vibration tests. This study uses a finite element model that includes water compressibility, and the model overpredicts the amount of radiation damping associated with the water. Until such matters can be resolved, the use of water compressibility in analyses can be questioned.

The foundation of the dam is taken as a finite region of massless rock, and so only its flexibility is included. Omission of foundation mass precludes any radiation of energy through the foundation away from the dam. However, force vibration testing typically shows a small amount of damping for a concrete dam, and this should include all radiation damping mechanisms. Further, the use of modal damping in an analytical model of a dam with a massless foundation (or equivalently, the use of mass and stiffness-proportional damping based on modal damping values) works well in many cases,[10] so this simpler and computationally less intensive approach is adopted here.

The foundation is modelled as linearly elastic, and so no abutment instabilities can occur. Such considerations can be important, such as at Pacoima Dam during the 1971 San Fernando and 1994 Northridge earthquakes,[11] and must be checked separately.

Approximations involved in the modelling of the opening and closing of contraction joints and cracks include a single shell element discretization in the thickness direction of the dam and smeared cracking. A scheme using several elements in the thickness direction connected by contact springs at a joint or crack would be more accurate but is computationally much more expensive. To compare the two procedures, the two-dimensional plane-strain beam problem of Figure 5(a) containing a centre joint and subjected to compressive force P and bending moment M is considered. Of interest are the contributions θ_J and U_J to the

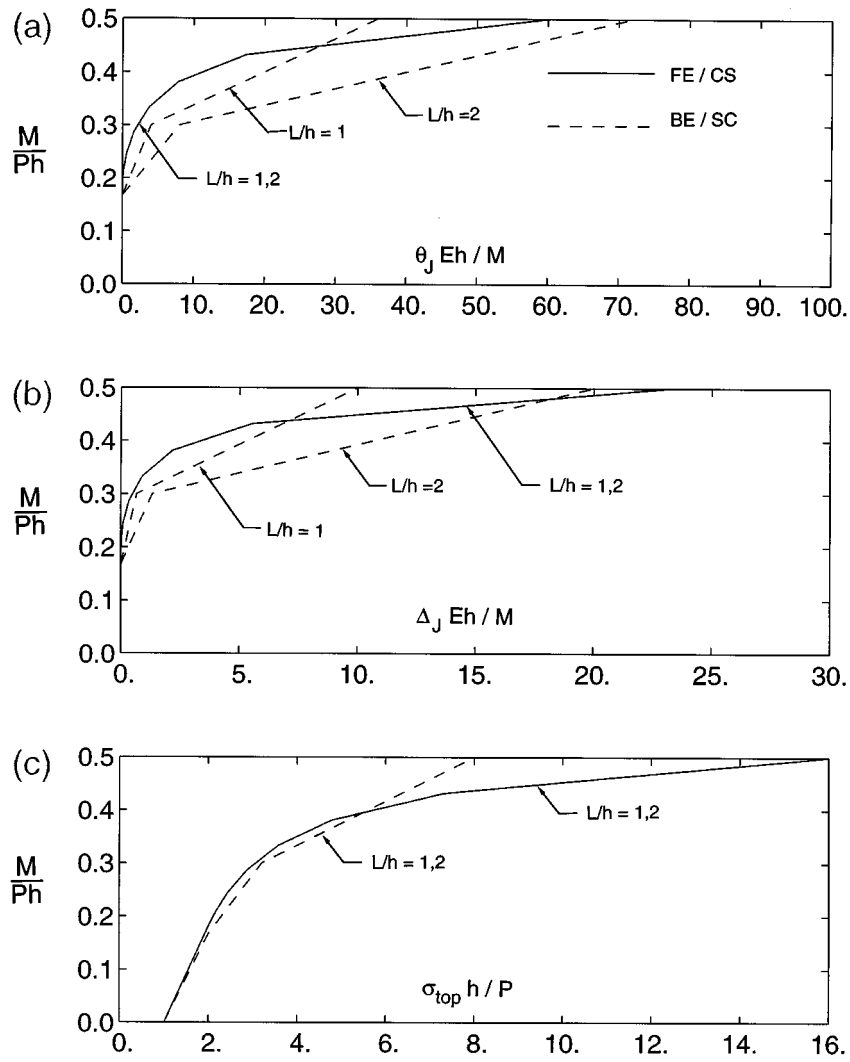

Figure 6. Results for the problem of Figure 5(a) using the finite element mesh with contact springs (FE/CS) shown in Figure 5(b) and the beam element with smeared cracking (BE/SC) shown in Figure 5(c): (a) rotation due to joint opening; (b) axial displacement due to joint opening; and (c) stress at top of joint

rotation and axial displacement, respectively, at a support caused by joint opening [see Reference 3 for details].

Results of the problem of Figure 5(a) are shown in normalized form in Figure 6: solid lines by the finite element mesh of Figure 5(b) with contact springs in the joint, and dashed lines by the single beam element with smeared cracking shown in Figure 5(c). This beam element is the plane-strain version of the shell element used in this paper and is representative of the behaviour of the shell element. The solid lines in Figure 6 should be close to the actual solutions of interest because the mesh of Figure 5(b) is relatively fine. For the beam element, the normalized joint displacements are proportional to L/h, as shown in Figures 6(a) and 6(b) for the two cases $L/h = 1$ and $L/h = 2$, which is fundamentally different from the actual behaviour. Nevertheless, the agreement is reasonable in the range $1 \leqslant L/h \leqslant 2$ which is typical of L/h in the upper part of an arch dam where the joint opening is the most important. Also shown in Figure 6 is the stress σ_{top} across the

top edge of the joint (Figure 6(c)) computed by the two procedures, and the agreement here is good except when the joint contact at the top reduces to a small value ($M/Ph \rightarrow 0{\cdot}5$). However, as $M/Ph \rightarrow 0{\cdot}5$, the true value of σ_{top} becomes unbounded, and so the stresses computed by the computer program at a joint edge ($\zeta = \pm 1$) should be interpreted as average values over the 1/8 depth tributary to a $\zeta = \pm 1$ integration point. Such stresses are probably more useful than large values resulting from a fine mesh in the vicinity of a stress singularity.

Orientation of the cracking planes is predetermined as the 1–3 plane in each element, which is close to being perpendicular to the cantilever bending stress. Although this seems reasonable, it should be noted that other orientations and patterns are possible, and the assumed one is not necessarily conservative.

Assumptions are also present in the sliding capability of the contraction joints and cracks. Sliding is assumed to be uncoupled for each of the three components, and this is thought to be a reasonable approximation. The option to provide keys for one or more shear components precludes any tangential motion in these components (perfect keys). In reality, however, some tangential motion will accompany the opening of a joint or crack (i.e. when the interlocking pieces have sloping sides such as do rough crack surfaces and bevelled keys).

Treatment of τ_{12} is somewhat *ad hoc* because contact conditions in both the joint and crack are relevant. Before cracking occurs, the term $\alpha_s \cdot G \cdot \gamma_{12}$ in equation (7c) prevents the stiffness of the 12 component from dropping to zero when the joint opens. Without this term, excessive sliding displacements can result. The $\alpha_s \cdot G \cdot \gamma_{12}$ term in equation (7c′) for the no-joint case plays a similar role after cracking takes place. Unfortunately, results are somewhat sensitive to the value of α_s.

The option to include water pressure in the contraction joints and cracks, which is based on the pressure in the reservoir at the upstream face of the dam, is very crude for the dynamic analysis. When a joint or crack closes and water is forced out, high pressures must be generated. However, no procedures to account for this action or to assess its importance are available.

As is evident, many assumptions have been introduced for a variety of practical reasons, and not all can be justified on the basis of their effects being small. However, it is felt that as experience is gained with the procedure, it will prove to be much more effective and realistic in the seismic assessment or design of an arch dam than the presently used linear analysis. Since the high artificial tensions of a linear analysis will not occur because of the joint opening and cantilever cracking capabilities, attention should focus on the magnitude of the compressive stresses, the amount of cracking, and the amplitudes of opening and sliding displacements.

3. SEISMIC RESPONSE OF A LARGE ARCH DAM

This study, which is condensed from Reference 4, demonstrates features of the formulation and documents some typical response characteristics of an arch dam. The particular dam considered here has a nearly full reservoir, and its geometry is similar to that of Pacoima Dam located in the San Gabriel Mountains north of Los Angeles. Use of these results to assess the seismic safety of Pacoima Dam must consider that this dam has a spillway tunnel 18 meters below the crest, and so the case analysed here corresponds to an unlikely simultaneous occurrence of flood and earthquake.

The dam is a 102 m high arch whose thickness at the crown section varies from 3·05 m at the crest to 27·4 m at the base. It is analysed here using the meshes of Figures 7 and 8. In the static analysis each of the six rows of dam elements is added by a construction step, and then the reservoir is filled to within 10·7 m of the crest (at the base of the top row of elements) in another five water-level steps. The dynamic analysis is conducted at this reservoir condition using a scaled-down version of the ground motions recorded above the left abutment of Pacoima Dam during the 1971 San Fernando earthquake (Figure 9). The same scale factor is applied to all three components of the ground motion to produce a peak acceleration of $0{\cdot}80g$. This peak acceleration occurs in the cross-stream component.

Particulars of the analysis are $\Delta t = 0{\cdot}001$ sec, $S_{min} = 0{\cdot}0$, $S_{max} = 0{\cdot}1$ (static analysis) or 0·01 (dynamic analysis), $\alpha_B = -0{\cdot}2$, $\gamma = 0{\cdot}70$ and $\beta = 0{\cdot}36$. The value for Δt resulted from a study as that value below which

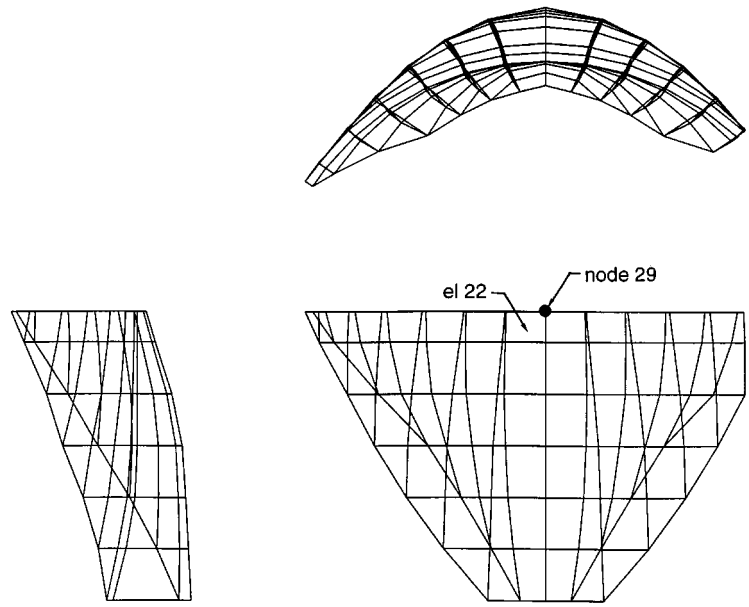

Figure 7. Finite element mesh of dam shown in plan (top), downstream elevation (bottom, right) and cross-stream elevation (bottom, left)

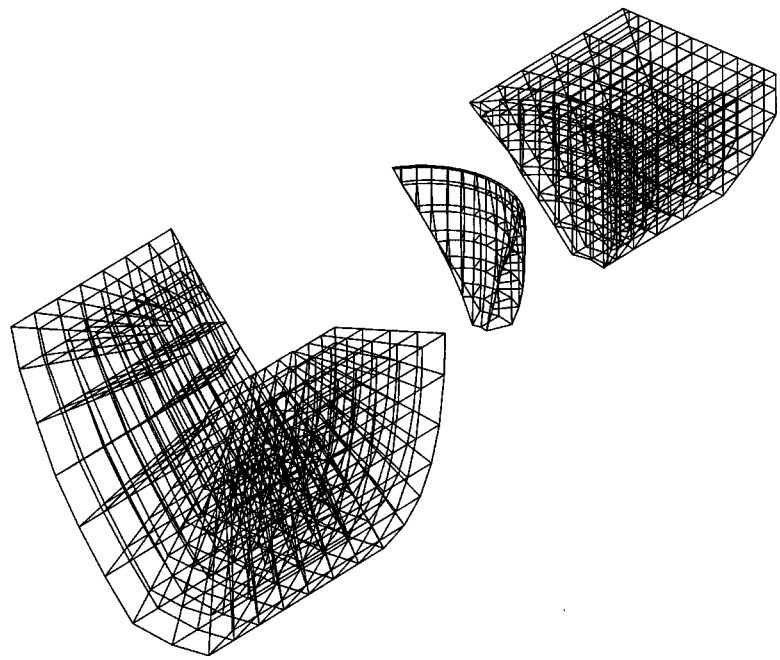

Figure 8. Foundation, dam and water meshes

no significant changes occurred in the results. Material properties for the dam are $E = 20\,700$ MPa, $v = 0{\cdot}20$, $\rho = 2{\cdot}40$ g/cm^3 (mass density), $\sigma_{\text{ten}} = 3{\cdot}8$ MPa, $\sigma_{\text{ten}}^{\text{red}} = 0{\cdot}1 \cdot \sigma_{\text{ten}}$, and $T_r = 0{\cdot}05$ sec. Keys are omitted for shear components 12 (in-plane shear) and 23 (crack shear) but included for shear component 13 (contraction-joint shear). Friction coefficients are $f_1 = 0{\cdot}50$ and $f_2 = 0{\cdot}75$. The shear retention coefficient is $\alpha_s = 0{\cdot}25$. Internal

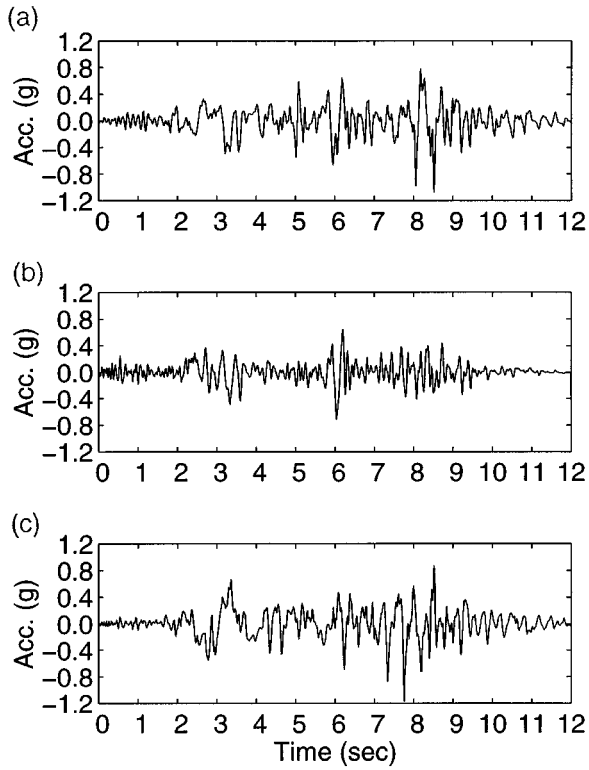

Figure 9. Ground motions recorded above the left abutment of Pacoima Dam during the 1971 San Fernando earthquake: (a) stream component; (b) vertical component; and (c) cross-stream component

water pressure is included. For the foundation, $E = 13\,800$ MPa and $v = 0{\cdot}25$. Stiffness and mass-proportional damping, computed to give 5% of critical at frequencies of 4 and 16 Hz, is used for the dam–foundation system. Fundamental frequencies of the linear dam–foundation system are 4·96 Hz for the stream-direction mode and 4·99 Hz for the cross-stream-direction mode.

The situation defined above is denoted as Case N1 and the corresponding linear case, obtained by removing the contraction joints and restraining cracking, as Case L1. Time histories of various responses for Case N1 are presented in Figure 10, and maximum values of arch compressive stress, joint opening, cantilever tensile stress, crack opening, and crack sliding (23 component) are shown in Figure 11. Each value listed corresponds to an element in the dam mesh and is the largest value from either the upstream or downstream face of the element. A cantilever tension of 3·8 MPa in Figure 11 indicates cracking. For Case N1, cracks occur in 8 elements, and maximum values are 3·5 cm for joint opening, 4·0 cm for crack opening, and 4·9 cm for crack sliding. The maximum compressive stress is 11·7 MPa.

Eleven other non-linear analyses were run as listed below (cases N2 to N12).

N2: $\Delta t = 0{\cdot}010$ sec
N3: $\Delta t = 0{\cdot}005$ sec
N4: $\Delta t = 0{\cdot}002$ sec
N5: water free-surface 65·5 m below the crest
N6: contraction-joint keys (13 component) removed
N7: $\alpha_s = 0{\cdot}00$
N8: $\alpha_s = 0{\cdot}50$

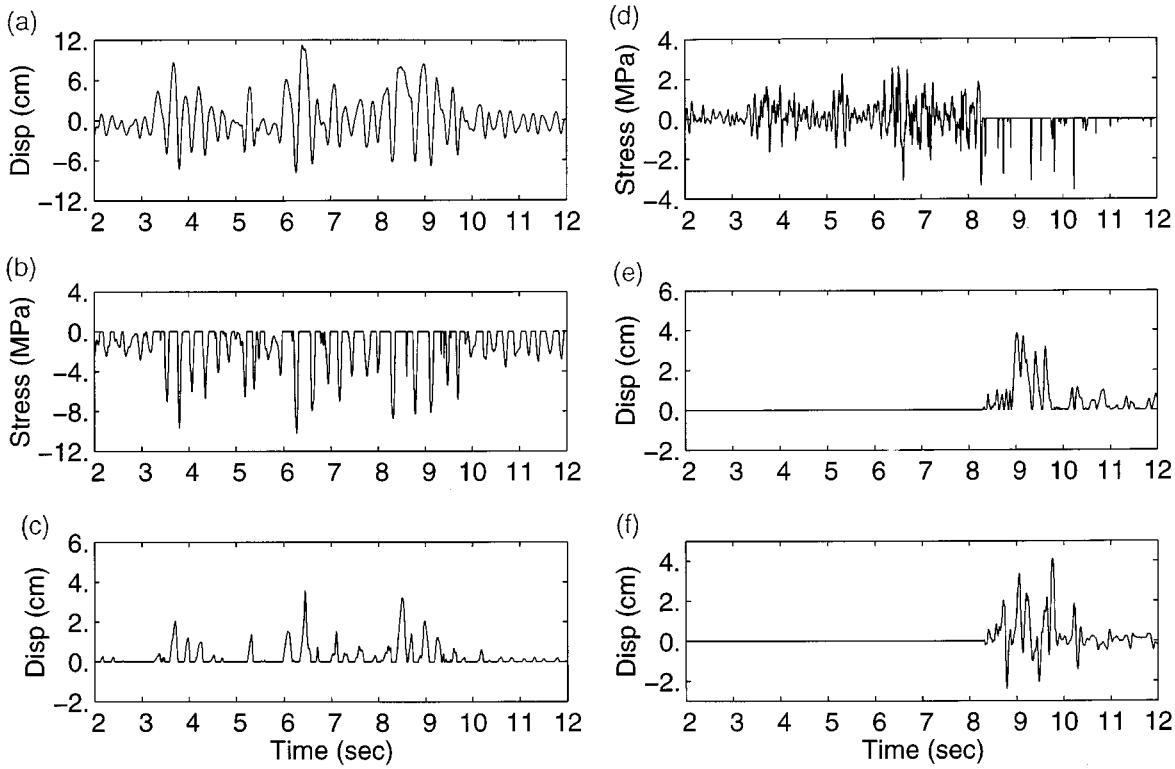

Figure 10. Selected time history responses for Case N1 nonlinear analysis: (a) stream displacement at node 29; (b) arch stress on upstream side of el 22; (c) joint opening on upstream side of el 22; (d) cantilever stress on downstream side of el 22; (e) crack opening on downstream side of el 22; and (f) crack sliding on downstream side of el 22

N9: peak ground acceleration scaled to 0·6*g*
N10: peak ground acceleration scaled to 1·0*g*
N11: internal water pressure omitted
N12: dam thickened in its upper portion to 12·2 m at the crest

All of these cases are modifications of Case N1 as indicated. Corresponding linear analyses (denoted by an L prefix) were also run. Results are summarized in Tables I and II. Note that Cases L1, L6, L7 and L8 are identical.

Sensitivity to the time step Δt, as revealed by Cases N1 to N4, owes to the cracking capability of the non-linear model. If a change in Δt is enough to cause an element previously on the verge of cracking to now crack, then significant differences in the response can result. In the non-linear analyses, the cracking response did not converge until Δt was reduced to 0·002 sec (Case N4), and thus reducing Δt to 0·001 sec (Case N1) produced little further change.

The results in Table I and II demonstrate the importance of various parameters. If the extent of cracking shown in Table II is chosen as an indicator of the severity of the damage, then the damage increases with higher water level, absence of keys in the contraction joints, lower value of α_s and (obviously) stronger ground motion. Results for $\alpha_s = 0$ (Case N7; see Reference 4) show that the dam elements slide away from the abutments, as indicated by larger joint openings there. This tends to overload the central cantilevers and produce more cracking, a tendency that is reduced in Cases N1 and N8 where α_s is greater than zero.

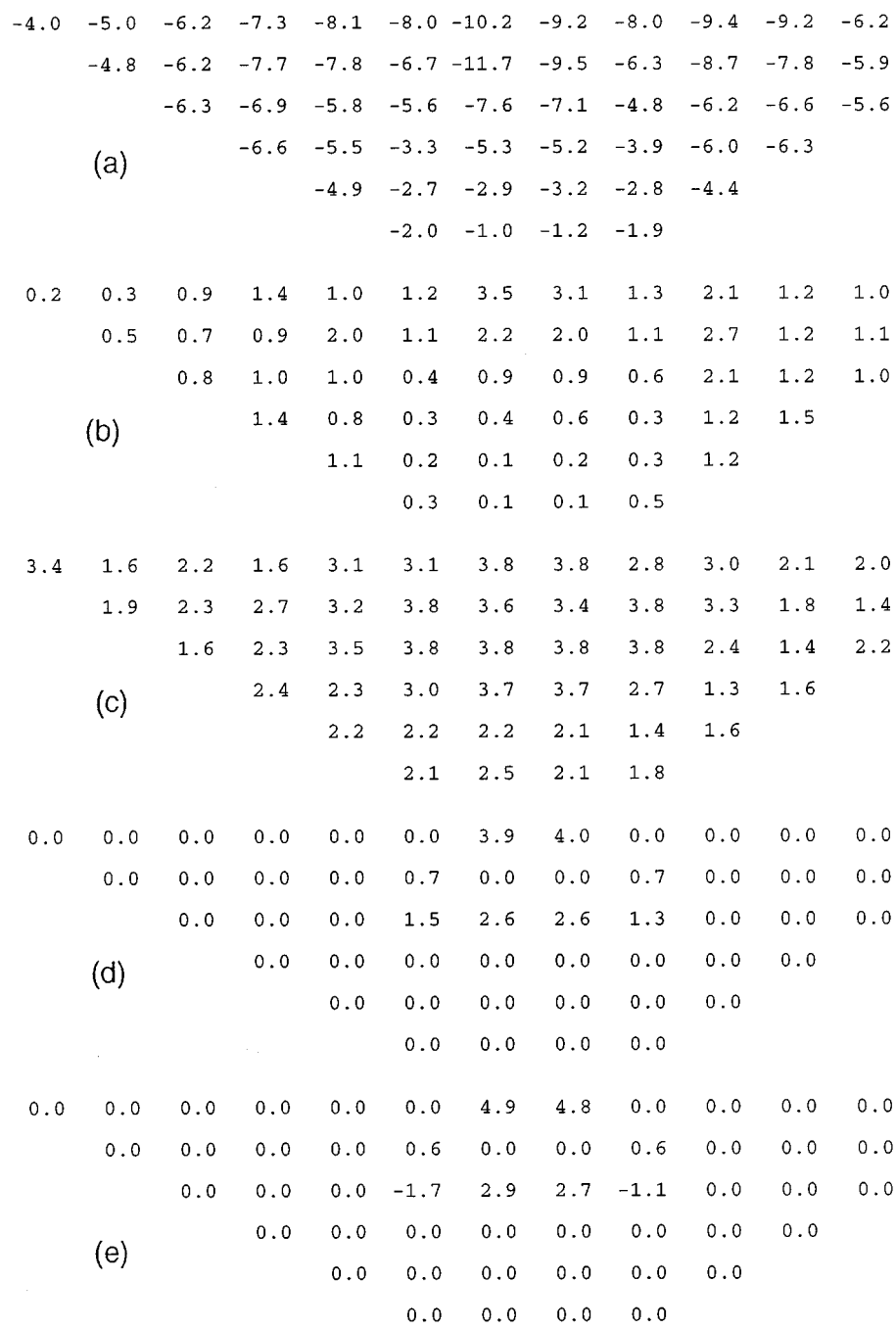

Figure 11. Distributions of maximum responses for Case N1 nonlinear analysis: (a) arch compression (MPa); (b) joint opening (cm); (c) cantilever tension (MPa); (d) crack opening (cm); and (e) crack sliding (cm)

Internal water pressure produces only small differences in the stresses in the linear model (L1 vs. L11 in Table I). However, this effect is enough to alter the cracking pattern in the non-linear model, which then leads to greater differences in the non-linear response (N1 vs. N11 in Table II).

Table I. Peak stresses in the dam for the linear cases

Case	Arch compression (MPa)	Arch tension (MPa)	Cantilever compression (MPa)	Cantilever tension (MPa)
L1,L6,L7,L8	−11·3	7·1	−5·3	5·0
L2	−11·0	6·7	−5·2	5·1
L3	−11·3	7·0	−5·2	5·1
L4	−11·3	7·1	−5·3	5·0
L5	−6·1	6·4	−3·2	3·3
L9	−8·7	5·0	−4·1	3·6
L10	−13·9	9·1	−6·5	6·3
L11	−11·2	7·2	−5·4	4·9
L12	−9·2	7·5	−7·2	3·9

Table II. Peak responses in the dam for the non-linear cases

Case	Arch compression (MPa)	Number of elements cracked	Joint opening (cm)	Joint sliding (cm)	Crack opening (cm)	Crack sliding (cm)
N1	−11·7	8	3·5	0·0	4·0	4·9
N2	−10·9	12	4·5	0·0	3·3	−3·1
N3	−11·5	9	3·7	0·0	2·7	2·9
N4	−11·7	8	3·5	0·0	4·0	4·4
N5	−8·0	2	2·7	0·0	0·6	−1·0
N6	−15·7	12	3·4	−11·8	3·2	−3·5
N7	−11·8	16	4·3	0·0	9·0	−12·7
N8	−14·4	7	5·0	0·0	4·6	8·0
N9	−9·4	4	2·3	0·0	2·7	−2·6
N10	−22·0	17	5·6	0·0	9·1	−6·7
N11	−11·8	9	2·9	0·0	2·9	−3·6
N12	−9·9	8	4·3	0·0	1·9	4·9

Thickening the dam in its upper portion (Case L12/N12) leads to less of an improvement in response than what might be expected, probably because of the additional mass. The extent of cracking is about the same.

In all of the analyses, the computer program shows that the dam survives, even for Case N10 where the response is quite severe. This does not mean that one should allow the dam to be operated with a 91 m water depth if the 1·0g earthquake is the ground motion to be considered. Judgment, with consideration of the points in Section 2·5, is required.

All of the analyses were run on a DEC 3000 Model 400 computer with a 100 MIPS processor. The non-linear analyses each took between 70 and 80 min of CPU time except that Cases N2, N3 and N4 with the longer time steps took 17, 25 and 42 min, respectively. Each linear analysis took 13 min with $\Delta t = 0{\cdot}001$ sec. The array storage required to run this problem was 1·11 million, and most of this was needed for the foundation.

4. CONCLUSIONS

The analysis procedure approximately accounts for many aspects of the seismic response of an arch dam, including cracking and the opening, closing and frictional sliding of cracks and joints. Economy of solution is

achieved using the smeared crack approach and an effective solution algorithm for the non-linear equations. Measures used to assess the results of the non-linear analysis include extent of cracking, amount of opening and sliding in joints and cracks, and amplitude of compressive stresses.

Engineering judgment is still required to decide safety issues because the computer program is unable to definitively establish conditions for water release. For example, an analysis of a large arch dam with nearly full reservoir subjected to strong shaking (1971 Pacoima Dam records scaled to 1·0g peak ground acceleration) shows the dam to remain stable. However, the significant extent of cracking, the maximum opening displacement of 9 cm, the maximum sliding displacement of 7 cm, and the maximum compressive stress of 22 MPa could be judged as being too extreme in a safety assessment. Conservatism is needed due to the limitations of the computer program, one of the most serious being the assumed orientation of the cracking planes. Reducing the ground motion to 0·8g peak acceleration makes the non-linear response values more acceptable.

The analysis procedure is efficient enough to make parameter studies practical. Such studies are essential because of the large number of parameters and because the inclusion of cracking makes the dam response sensitive to values of these parameters.

REFERENCES

1. (a) G. L. Fenves, S. Mojtahedi and R. B. Reimer, 'ADAP-88, A computer program for nonlinear earthquake analysis of concrete arch dams', *Report No. UCB/EERC 89/12*, Earthquake Engineering Research Center, University of California at Berkeley, November 1989. (b) G. L. Fenves, S. Mojtahedi and R. B. Reimer, 'Parameter study of joint opening effects on earthquake response of arch dams', *Report No. UCB/EERC-92/05*, Earthquake Engineering Research Center, University of California at Berkeley, April 1992.
2. J.-M. Hohberg, 'A joint element for the nonlinear dynamic anlaysis of arch dams', *Report No. 186*, Institute of Structural Engineering, ETH, Zurich, July 1992.
3. M. J. Dowling, 'Nonlinear seismic analysis of arch dams', *Report No. EERL 87-03*, Earthquake Engineering Research Laboratory, Caltech, Pasadena, CA, 1987.
4. J. F. Hall, 'Efficient nonlinear seismic analysis of arch dams, User's manual for SCADA', *Report No. EERL 96-01*, Earthquake Engineering Researh Laboratory, Caltech, Pasadena, CA, 1996 (modified July 1997).
5. K. J. Bathe, *Finite Element Procedures in Engineering Analysis*, Prentice-Hall, Englewood Cliffs, NJ, 1982.
6. D. D. Adams and W. L. Wood, 'Comparison of Hilber–Hughes–Taylor and Bossak 'α-methods' for the numerical integration of vibration equations', *Int. J. Numer. Meth. Engng.* **19** (1983).
7. California Division of Mines and Geology, 'CSMIP strong-motion records from the Northridge, California earthquake of January 17, 1994', *Report OSMS 94-07.*
8. P. S. Nowak, 'Effect of nonuniform seismic input on arch dams', *Report No. EERL 88-03*, Earthquake Engineering Research Laboratory, Caltech, Pasadena, CA, 1988.
9. Z. H. Duron, 'Experimental and finite element studies of a large arch dam', *Report No. EERL 87-02*, Earthquake Engineering Research Laboratory, Caltech, Pasadena, CA, 1987.
10. J. F. Hall, 'The dynamic and earthquake behavior of concrete dams: Review of experimental behavior and observational evidence', *Soil Dyn. Earthquake Engng.* **7** (1988).
11. Earthquake Engineering Research Institute, 'Northridge earthquake reconnaissance report', Vol. 1, *Earthquake Spectra*, Suppl. C, Vol. 11, April 1995.

